nature sustainability

SUPPLEMENTARY INFORMATION

https://doi.org/10.1038/s41893-018-0168-z

In the format provided by the authors and unedited.

Quantifying resilience to recurrent ecosystem disturbances using flow–kick dynamics

Katherine Meyer[1*], Alanna Hoyer-Leitzel[2], Sarah Iams[3], Ian Klasky[4], Victoria Lee[5], Stephen Ligtenberg[5], Erika Bussmann[6] and Mary Lou Zeeman[5]

[1]University of Minnesota, Minneapolis, MN, USA. [2]Mount Holyoke College, South Hadley, MA, USA. [3]Harvard University, Cambridge, MA, USA. [4]University of Colorado, Boulder, CO, USA. [5]Bowdoin College, Brunswick, ME, USA. [6]Minnetonka High School, Minnetonka, MN, USA. *e-mail: meye2098@umn.edu

Supplementary Tables

Supplementary Table 1
Connecting some common vocabularies from the ecology, mathematics, and resilience literatures

IDEA	ECOLOGY	MATH	RESILIENCE
General system disruption	perturbation[19,20]	perturbation	disturbance[6,21] change[6,21]
Discrete perturbation to system state	disturbance event[18,19]	kick[29] impulse[30]	disturbance event[21] pulse disturbance[21]
Magnitude of discrete perturbation	magnitude[19] - intensity[18,19] - severity[18,19]	kick magnitude	magnitude, severity[21]
System behaviour between perturbations	trajectory[26]	flow[34]	response[6] recovery[21]
Time interval between perturbations	return interval[18,19] recurrence interval[19] disturbance interval[26]	flow time	time for recovery[21]
System states that share a fundamental structure	ecological regime	basin of attraction domain of attraction	regime[6,21,31] domain of attraction[7]

Supplementary Methods

Here we present some mathematical arguments that underpin our work. Figure S1 portrays a general one-dimensional flow-kick system that we use to frame many of our results.

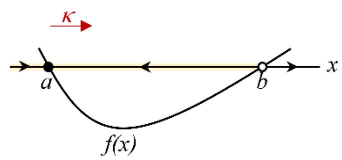

Supplementary Figure 1 A general one-dimensional flow-kick system (see text for details).

In this context, the ordinary differential equation $x' = f(x)$, where x' denotes dx/dt, dictates the undisturbed dynamics. We assume throughout that f is sufficiently differentiable (e.g. C^1). For a flow time τ and kick size κ, the flow-kick map is defined by $G_{\tau,\kappa}(x) = \varphi_\tau(x) + \kappa$, where $\varphi_\tau(x)$ is the flow generated by vector field f [34]. We focus on the resilience of the basin of attraction, $\mathcal{B}(a)$, of the attracting equilibrium a to kicks $\kappa > 0$. These kicks counteract the undisturbed dynamics, which flow for time τ toward attracting equilibrium a and away from repelling equilibrium b (the relevant boundary of $\mathcal{B}(a)$).

We refer to this case with $a < b$, $f(x) < 0$ on (a,b), $f'(a) < 0$, $f'(b) > 0$, and $\kappa > 0$ as *the hypotheses of Figure S1*. Note that rotation of Figure S1 by 180 degrees yields a picture in which $a > b$, $f(x) > 0$ on (a,b), $f'(a) < 0$, $f'(b) > 0$, and $\kappa < 0$; arguments that use the hypotheses of Figure S1 could be easily modified to handle this alternate case.

Several results below rely on the following fact.

Lemma 1: A one dimensional flow-kick map $G_{\tau,\kappa}$ is monotone.

Proof: Suppose $x < y$. Then monotonicity of flow on a one-dimensional space implies

$\varphi_\tau(x) < \varphi_\tau(y)$. Adding the same kick to both sides preserves the inequality: $\varphi_\tau(x) + \kappa < \varphi_\tau(y) + \kappa$. Hence $G_{\tau,\kappa}(x) < G_{\tau,\kappa}(y)$. //

1. Plotting the flow-kick resilience boundary based on minimum recovery times

Definition: The flow-kick resilience boundary, R, for the basin of attraction of a, $\mathcal{B}(a)$, separates disturbance patterns (τ, κ) for which the flow-kick trajectory of a remains in $\mathcal{B}(a)$ from disturbance patterns for which the flow-kick trajectory of a escapes from $\mathcal{B}(a)$.

Proposition 1**:** In addition to the hypotheses of Figure S1, suppose that f is unimodal between a and b. Then a disturbance (τ, κ) belongs to the flow-kick resilience boundary R for the basin of a exactly when τ is the minimum time in which the system can recover by $-\kappa$, taken over all possible intervals of length $|\kappa|$ between a and b.

Proof: Unimodality of the vector field function guarantees a unique interval of length $|\kappa|$ over which the minimum flow time, m, occurs; call it $[y - \kappa, y]$. Geometrically, the interval $[y - \kappa, y]$ corresponds to 'slicing' a cap of width κ off the bottom of the graph of f, since that corresponds to the fastest flow rates. If τ is greater than m, then a flow-kick trajectory that starts at a will not escape from the basin of attraction of a. This is because $\tau > m$ implies $\varphi_\tau(y) < y - \kappa$, so $G_{\tau,\kappa}(y) < y$; monotonicity of the 1D flow-kick map (Lemma 1) then implies $\mathrm{G}^n_{\tau,\kappa}(a) < \mathrm{G}^n_{\tau,\kappa}(y) < y < b$ for all n. On the other hand, if τ is less than m, then for any x in $[a, b]$ we have $\varphi_\tau(x) > x - \kappa$ so $G_{\tau,\kappa}(x) > x$. Compactness of $[a,b]$ guarantees the existence of an ε such that $G_{\tau,\kappa}(x) - x > \varepsilon > 0$ for each x in $[a, b]$ and so a flow-kick trajectory starting at a escapes from the basin of attraction of a within j flow-kick iterations where j is the smallest integer greater than $(b - a)/\varepsilon$. Hence $(\tau = m, \kappa)$

lies on the flow-kick resilience boundary between disturbance patterns for which the flow-kick trajectory of *a* escapes from $\mathscr{B}(a)$ and disturbance patterns for which the flow-kick trajectory of *a* remains in $\mathscr{B}(a)$. //

2. Determining finite area of the "nonresilient" region

Recall that the nonresilient region of disturbance space, denoted *N* (see Figure 2b), is the subset of disturbance space with $\tau > 0$ that lies above the flow-kick resilience boundary *R* and below the horizontal asymptote at $\kappa = |a - b|$

Proposition 2. Under the hypotheses of Figure S1, the area of the nonresilient region, *N*, is finite.

Proof: We first show that the region *N* has finite area when the vector field for the undisturbed system is a quadratic function $q(x)=r(x-a)(x-b)$ with $r > 0$. For any kick κ between 0 and $b - a$, symmetry of the parabola $y=q(x)$ implies that the shortest time in which the system can recover by $-\kappa$ between *a* and *b* occurs over an interval of length κ centered on $(a+b)/2$. Separation of variables applied to $x'=q(x)$ yields this minimum recovery time as a function of κ:

$$\tau = F(\kappa) = \int_{\frac{a+b+\kappa}{2}}^{\frac{a+b-\kappa}{2}} \frac{dx}{r(x-a)(x-b)}.$$

The flow-kick resilience boundary is composed of points $(F(\kappa), \kappa)$ (see section S1). Integrating and solving for κ in terms of τ yields a function for the boundary:

$$\kappa = (b-a)\tanh\frac{r(b-a)\tau}{4}.$$

The area of the nonresilient region, *N*, is then

$$\lim_{T\to\infty} \int_0^T (b-a)\left(1 - \tanh\left(\frac{r(b-a)\tau}{4}\right)\right) d\tau$$

$$= (b-a) \lim_{T\to\infty} \left(T - \frac{\ln(\cosh(CT))}{C}\right) \quad \text{(where} \quad C = \frac{r(b-a)}{4}\text{)}$$

$$= (b-a) \lim_{T\to\infty} \left(T - \frac{\ln\left(\frac{e^{C\tau}+e^{-CT}}{2}\right)}{C}\right)$$

$$= (b-a) \lim_{T\to\infty} \left(T - \frac{\ln\left(\frac{e^{CT}}{2}\right)}{C}\right) \qquad \text{(since } e^{-CT} \to 0 \text{ as } T \to \infty\text{)}$$

$$= \frac{(b-a)\ \ln 2}{C}$$

$$= \frac{4 \ln 2}{r},$$

a finite quantity.

The proposition then follows from the facts that

(i) by choosing r small enough, we may ensure that $0 < q(x) < f(x)$ for all x in (a,b), and

(ii) if $0 < q(x) < f(x)$ for all x in (a,b), then the nonresilient region for $x' = f(x)$ is a subset of the nonresilient region for $x' = q(x)$. //

When approximating the finite area of a nonresilient region, fact (ii) can yield an analytic bound on the tail of the improper integral. For example, if $f(x) = x\left(1 - \frac{x}{100}\right)\left(\frac{x}{20} - 1\right)$, the quadratic function $q(x) = 20\left(1 - \frac{x}{100}\right)\left(\frac{x}{20} - 1\right)$ satisfies $0 < q(x) < f(x)$ on (20, 100). As in the proof of Proposition 2, we can analytically determine both the flow-kick resilience boundary for $x' = q(x)$ (here, $\kappa(\tau) = 80 \tanh(\tau/5)$) and the improper integral $I = \int_{\tau_0}^{\infty}(80 - 80\tanh\frac{\tau}{5})d\tau$. Since the nonresilient region of $x' = q(x)$ is a subset of that of $x' = f(x)$, the area of the region between the flow-kick resilience boundary for the cubic system and the horizontal asymptote over the tail $\tau > \tau_0$ can be no larger than I.

3. Connecting the distance-to-bifurcation resilience metric to the slope of the flow-kick resilience boundary near the origin.

To understand the relationship between the slope of the flow-kick resilience boundary near the origin and the distance to bifurcation in the undisturbed system $x' = f(x)$, we first need the following fact.

Proposition 3. If the flow time τ and kick κ in a flow-kick system based on an undisturbed system $x' = f(x)$ are held in a constant ratio $\kappa/\tau = r$, then, in the limit as τ goes to zero the flow-kick system limits to the continuous system $x' = f(x)+r$.

Proof: At any point x in state space, the flow map is $\varphi_\tau(x) = x + \tau f(x) + O(\tau^2)$, where O is the big-O Landau symbol representing terms of order τ^2 and higher. The flow-kick map is thus $G_{\tau,\kappa}(x) = x + \tau f(x) + O(\tau^2) + \kappa$, and since $\kappa/\tau = r$, this is $G_{\tau,\kappa}(x) = x + \tau f(x) + r\tau + O(\tau^2)$. Rearranging terms gives

$$\frac{G_{\tau,\kappa}(x) - x}{\tau} = f(x) + r + O(\tau)$$

Taking the limit as τ goes to zero yields

$$\lim_{\tau \to 0} \frac{G_{\tau,\kappa}(x) - x}{\tau} = \lim_{\tau \to 0}\big(f(x) + r + O(\tau)\big)$$

The left side of this equation represents the vector field generated by the infinitesimal flow-kick map, while the right side simplifies to $f(x)+r$, as claimed. //

Now we introduce a parameter μ to the underlying system. So $x' = f(x) + \mu$, and when $\mu = 0$, $f(x)$ has attracting and repelling equilibria at a and b, respectively, as in Figure S1.

Corollary 3.1 If the underlying one-parameter system $x'=f(x)+\mu$ has a saddle-node bifurcation at $\mu=\mu^*>0$, at which the attracting and repelling equilibria corresponding to a and b coalesce and disappear, then the slope $dR/d\tau$ of the flow-kick resilience boundary $R(\tau)$ converges to μ^* *as* τ approaches 0.

Proof: Proposition 3 implies that by choosing small enough τ and κ along the line $\kappa=r\,\tau$ in (τ, κ) space, trajectories of the flow kick system $x_{n+1} = G_{\tau,\kappa}(x_n)$ can be arbitrarily well-approximated by those of the continuous system $x'=f(x)+r$. If $\mu_1< \mu^*$, then trajectories of flow-kick systems for f with disturbance patterns approaching the origin along the line $\kappa= \mu_1 \tau$ in (τ, κ) space become arbitrarily close to those of $x'= f(x)+ \mu_1$. This system retains an attracting equilibrium in $[a,b]$. Thus, for sufficiently small τ and κ with $\kappa= \mu_1 \tau$, (τ, κ) lies below R in the "resilient" region of (τ, κ) space. On the other hand, if $\mu_2>\mu^*$, then trajectories of flow-kick systems approaching the origin along the line $\kappa= \mu_2 \tau$ become arbitrarily well-approximated by those of $x'=f(x)+ \mu_2$. This system has lost the attracting equilibrium, and all trajectories escape from $[a,b]$. Thus, for sufficiently small τ and κ with $\kappa= \mu_2 \tau$, (τ, κ) lies above R in the "nonresilient" region of (τ, κ) space. As the borderline between these two cases, the flow-kick resilience boundary $R(\tau)$ must have a slope limiting to μ^* as τ approaches zero. //

4. Extending deterministic results to predict outcomes of stochastic disturbances

The following propositions formalize and generalize to one dimensional systems the statements that if τ and κ are drawn from a bounded rectangular subset either entirely below or entirely above the flow-kick resilience boundary (e.g. the solid- or dashed-edged boxes in Figure 2b), then randomized flow-kick trajectories starting at the attracting equilibrium will stay within its basin of attraction indefinitely or escape in finite time, respectively.

Proposition 4. In addition to the hypotheses of Figure S1, suppose that for each disturbance in the rectangle $\{(\tau,\kappa)$: $0<\tau_1\leq \tau \leq \tau_2$, $0<\kappa_1\leq \kappa \leq \kappa_2\}$ the deterministic flow-kick trajectory $\{a, \mathrm{G}_{\tau,\kappa}(a), \mathrm{G}^2_{\tau,\kappa}(a), \dots\}$ remains bounded in the interval $[a,b]$. Then if kicks K and recovery periods T vary stochastically but satisfy $\kappa_1 \leq K \leq \kappa_2$ and $\tau_1 \leq T \leq \tau_2$, any resulting flow-kick trajectory that starts at a also stays within $[a,b]$.

***Proof*:** An inductive argument (below) shows that after $n \geq 0$ iterations of the flow-kick map,

$$\mathrm{G}^n_{\tau_2,\kappa_1}(a) \leq \mathrm{G}^n_{T,K}(a) \leq \mathrm{G}^n_{\tau_1,\kappa_2}(a).$$

Since by assumption $a \leq \mathrm{G}^n_{\tau_2,\kappa_1}(a)$ and $\mathrm{G}^n_{\tau_1,\kappa_2}(a) \leq b$, we have that for all $n \geq 0$

$$a \leq \mathrm{G}^n_{T,K}(a) \leq b,$$

as desired.

The induction proceeds on iterations n of the flow-kick map. In the first flow, (because a is an equilibrium of the flow) we have $\varphi_{\tau_2}(a) = \varphi_T(a) = \varphi_{\tau_1}(a) = a$, and after the first kick $\varphi_{\tau_2}(a) + \kappa_1 \leq \varphi_T(a) + K \leq \varphi_{\tau_1}(a) + \kappa_2$, establishing the base case $\mathrm{G}_{\tau_2,\kappa_1}(a) \leq \mathrm{G}_{T,K}(a) \leq \mathrm{G}_{\tau_1,\kappa_2}(a)$.

Now for any $m>0$, if $\mathrm{G}^m_{\tau_2,\kappa_1}(a) \leq \mathrm{G}^m_{T,K}(a) \leq \mathrm{G}^m_{\tau_1,\kappa_2}(a)$, monotonicity of the flow implies that $\varphi_{\tau_2}\left(\mathrm{G}^m_{\tau_2,\kappa_1}(a)\right) \leq \varphi_T\left(\mathrm{G}^m_{T,K}(a)\right) \leq \varphi_{\tau_1}\left(\mathrm{G}^m_{\tau_1,\kappa_2}(a)\right)$, while the ordering of the kicks implies

$\varphi_{\tau_2}\left(\mathrm{G}^m_{\tau_2,\kappa_1}(a)\right) + \kappa_1 \leq \varphi_T\left(\mathrm{G}^m_{T,K}(a)\right) + K \leq \varphi_{\tau_1}\left(\mathrm{G}^m_{\tau_1,\kappa_2}(a)\right) + \kappa_2$. This is equivalent to

$\mathrm{G}^{m+1}_{\tau_2,\kappa_1}(a) \leq \mathrm{G}^{m+1}_{T,K}(a) \leq \mathrm{G}^{m+1}_{\tau_1,\kappa_2}(a)$, completing the inductive step. //

Proposition 5. In addition to the hypotheses of Figure S1, suppose that for fixed τ and κ the deterministic flow-kick trajectory $\{a, \mathrm{G}_{\tau,\kappa}(a), \mathrm{G}^2_{\tau,\kappa}(a), \dots\}$ exceeds b in finite time $t_{\tau,\kappa}$. Then if kicks K and recovery periods T vary stochastically but satisfy $\kappa \leq K$ and $T \leq \tau$, any resulting flow-kick trajectory that starts at $x=a$ also leaves $[a,b]$ in finite time.

Proof: As in the proof of Proposition 4, we have that

$$\mathrm{G}^n_{\tau,\kappa}(a) \leq \mathrm{G}^n_{T,K}(a).$$

Since the trajectory $\left\{\mathrm{G}^n_{\tau,\kappa}(a)\right\}_{n=0}^{\infty}$ exceeds b in finite time, so does any realized trajectory $\left\{\mathrm{G}^n_{T,K}(a)\right\}_{n=0}^{\infty}$. //

Corollary 5.1 If in addition to the hypotheses of Figure S1, for each τ and κ in the rectangular domain $D = \{(\tau,\kappa) : 0 \leq \tau_1 \leq \tau \leq \tau_2,\ 0 \leq \kappa_1 \leq \kappa \leq \kappa_2\}$ the deterministic flow-kick trajectory $\{a, \mathrm{G}_{\tau,\kappa}(a), \mathrm{G}^2_{\tau,\kappa}(a), \ldots\}$ exceeds b in finite time $t_{\tau,\kappa}$, then if kicks K and recovery periods T are drawn stochastically from D, any resulting flow-kick trajectory that starts at $x=a$ also leaves $[a,b]$ in finite time.

5. Calculating flow-kick equilibria via Newton's method

Newton's method was implemented in the MATLAB code *Newton.m* to find zeros of $F(x) = G_{\tau,\kappa}(x) - x$ for fixed values of τ and κ. The iterated step in this algorithm is

$$x_{n+1} = x_n - \frac{\mathrm{G}_{\tau,\kappa}(x_n) - x_n}{D_x\left(\mathrm{G}_{\tau,\kappa}(x) - x\right)|_{x=x_n}} = x_n - \frac{\mathrm{G}_{\tau,\kappa}(x_n) - x_n}{D_x(\mathrm{G}_{\tau,\kappa}(x))|_{x=x_n} - 1} \qquad (1)$$

The term $D_x\left(\mathrm{G}_{\tau,\kappa}(x)\right)|_{x=x_n}$ in (1) simplifies to $D_x\left(\varphi_\tau(x)\right)|_{x=x_n}$ because $G_{\tau,\kappa}(x) = \varphi_\tau(x) + \kappa$, with κ constant. The spatial (x) derivative of the flow function $\varphi_\tau(x)$ corresponding to the vector field $f(x)$ relates closely to the solution of the variational equation

$$du/dt = [D_x(f)|_{x(t)}]\, u \qquad (2)$$

which for initial condition $u=u_0$ is[1] $u(t)=D_x[\varphi_t]\, u_0$ with the derivative $D_x[\varphi_t]$ evaluated at $x=x_0$. When computing Newton iterates, it is natural to couple the evolution of x by $x'=f(x)$ with the evolution of u by equation (2); the code *CoupledVar.m* contains these coupled ODEs. By numerically solving the variational equation for $u(\tau)$ with $u_0=1$ *and* $x_0=x_n$, we obtained the desired term $D_x(\varphi_\tau(x))|_{x=x_n}$ for each step in the algorithm (1).

6. Analyzing stability of flow-kick equilibria

Proposition 6: Suppose x^* is an equilibrium for the flow-kick map $G_{\tau,\kappa}$ in a one-dimensional system and let f be the continuously differentiable vector field for the undisturbed dynamics. Let $x(t)$ represent the flow trajectory from x^* to $x^*-\kappa$. If $\int_0^\tau [D_x(f)|_{x(t)}]\, dt$ is negative, then x^* is a stable flow-kick equilibrium; if $\int_0^\tau [D_x(f)|_{x(t)}]\, dt$ is positive, then x^* is an unstable flow-kick equilibrium.

Proof: The linearization of the flow-kick map about the equilibrium x^* is the map sending y to $(D_x G_{\tau,\kappa}|_{x=x^*})\, y$, where $y=x-x^*$. Note that $D_x G_{\tau,\kappa}|_{x=x^*} = D_x(\varphi_\tau(x)+\kappa)|_{x=x^*} = D_x\, \varphi_\tau\, |_{x=x^*}$

since κ is constant. As in the previous section, the spatial (x) derivative of the flow function $\varphi_\tau(x)$ corresponding to the vector field $f(x)$ relates closely to the solution of the variational equation

$$du/dt = [D_x(f)|_{x(t)}]\, u \qquad (2)$$

where $x(t)=\varphi_t(x_0)$ (i.e. the derivative $D_x(f)$ is computed along the trajectory from x_0). Namely, the solution to the variational equation (1) with initial condition $u(0)=u_0$ is[34]

$$u(t) = \left(D_x(\varphi_t)|_{x=x_0}\right) u_0\ . \qquad (3)$$

Therefore, the desired derivative $D_x\varphi_\tau|_{x=x^*}$ is precisely the solution $u(\tau)$ to the variational equation (2) at time τ with initial condition $u_0 = 1$ and x-trajectory starting at $x_0 = x^*$. In a one-dimensional system, one can solve (2) for $u(\tau)$ analytically via separation of variables:

$$\frac{du}{u} = [D_x(f)|_{x(t)}]\, dt$$

$$\int_{u(0)=1}^{u(\tau)} \frac{du}{u} = \int_0^\tau [D_x(f)|_{x(t)}]\, dt$$

$$\ln\big(u(\tau)\big) - \ln\big(u(0)\big) = \int_0^\tau [D_x(f)|_{x(t)}]\, dt$$

$$u(\tau) = \exp\Big(\int_0^\tau [D_x(f)|_{x(t)}]\, dt\Big).$$

If $\int_0^\tau [D_x(f)|_{x(t)}]\, dt$ is negative, then $u(\tau) = D_x\varphi_\tau|_{x=x^*}$ is less than one, so the linearized flow-kick map has eigenvalue less that one, and x^* is a stable flow-kick equilibrium; if $\int_0^\tau [D_x(f)|_{x(t)}]\, dt$ is positive, then $u(\tau) = D_x\varphi_\tau|_{x=x^*}$ is greater than one and x^* is an unstable flow-kick equilibrium. //

Corollary 6.1: In the special case that $D_x(f)$ is negative (positive)—or equivalently, the potential function $V = -\int f\, dx$ is concave up (down)—over the entire flow-kick equilibrium interval, the sign of the integral $\int_0^\tau [D_x(f)|_{x(t)}]\, dt$ and hence the stability (instability) of x^* can be determined by inspection.

7. Viewing the flow-kick resilience boundary as a bifurcation curve

So far, we have calculated flow-kick resilience boundaries in terms of minimum recovery times (see section 1). However, the resilience boundaries of the fishery and lake water quality examples can also be viewed as bifurcation curves at which stable and unstable flow-kick equilibrium intervals coalesce and disappear.

Supplementary Figure 2 illustrates this interpretation for the lake water quality example with undisturbed dynamics $\frac{dx}{dt} = l - sx + \frac{rx^q}{m^q+x^q}$. Panel a shows that when κ =10 and τ=2, there are three flow-kick equilibrium intervals: A and C (stable), and B (unstable). The bifurcation diagram in panel b shows how the existence and positions of the flow-kick equilibria vary with κ while τ=2 remains fixed. For each value of κ, a vertical slice shows the locations of flow-kick equilibrium intervals, bounded by the grey curve below and the black curve above. The particular case κ=10 is highlighted as an example. As κ approaches a critical magnitude $\kappa^* \approx 15$, the stable and unstable low-P equilibrium intervals overlap, and at $\kappa = \kappa^*$ they coalesce and disappear in a saddle-node bifurcation. For $\kappa > \kappa^*$, there is a single, globally attracting equilibrium interval at high P. If x starts near the deterministic equilibrium a, a succession of kicks that occurs every 2 time units will escape the basin of attraction of a if $\kappa > \kappa^*$, or will stay in the basin if $\kappa > \kappa^*$. The pair (2, κ^*) thus belongs on the flow-kick resilience boundary for this system.

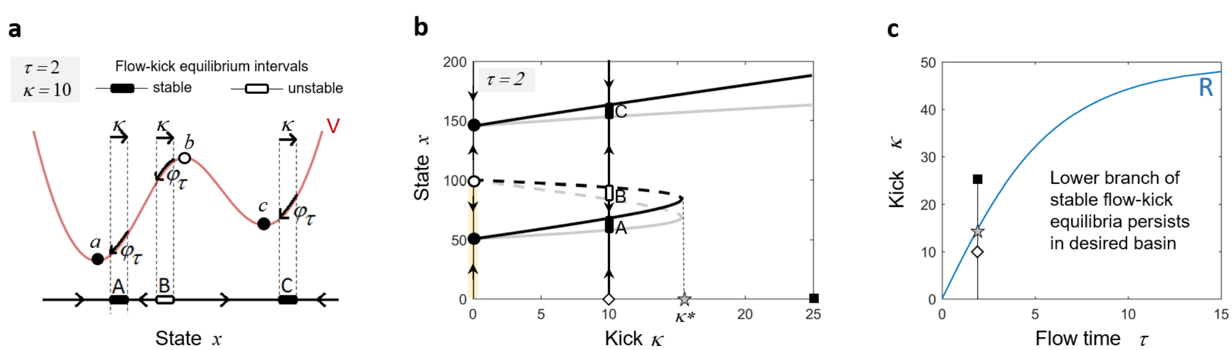

Supplementary Figure 2 The resilience curve as a bifurcation diagram. (see text for details).

Panel c of Supplementary Figure 2 generalizes a step further by allowing the recovery time τ to vary (horizontal axis) and plotting (solid curve R) the kick size κ (now on the vertical axis) at which the saddle-node bifurcation occurs. The vertical line at $\tau = 2$ corresponds to the horizontal axis of the bifurcation diagram in panel b. The curve R of bifurcation values separates disturbance patterns (τ, κ) that maintain the structure of two, alternative stable equilibrium intervals (below) from disturbance patterns for which the lower stable equilibrium interval is lost (above). R is precisely our flow-kick resilience boundary in disturbance space for the basin of the underlying deterministic attractor a.

The flow-kick equilibria in Supplementary Figure 2a were calculated using Newton's method (MATLAB codes *Newton.m* and *CoupledVar.m*, section 5); their stability can be deduced from Corollary 6.1 (section 6). The branches of equilibria in Supplementary Figure 2b were calculated using the MATLAB script *Branch.m*, which calls *Newton.m*.

Supplementary Discussion

1. Landscape Disturbance

Here we discuss how the flow-kick modeling framework both relates to and departs from foundational landscape models of disturbance regimes developed by Turner and colleagues[26] and Fraterrigo and Rusak[27], herein referred to as successional patch models. A successional patch model represents the landscape as a grid (Supplementary Figure 3a), and in the absence of disturbances each patch in the grid progresses linearly through successional stages (Supplementary Figure 3b). A uniform, mature landscape is therefore the attracting state for the system without disturbances. Disturbance events reset succession to stage one over randomly positioned subsets of the grid (e.g. lightest square, Supplementary Figure 3a). By normalizing temporal and spatial variables, successional patch models have helped shape our understanding of the role of scale in landscape dynamics and the impact of disturbance extent and frequency on landscape heterogeneity and variance.

In addition to identifying patterns of heterogeneity and variance, Turner and colleagues[26] point out a possibility beyond the scope of their model: that large and frequent disturbances could trigger a regime shift. In their words (p. 220),

> "Under conditions of large frequent disturbance, one of the most interesting possibilities is the potential for unstable or catastrophic change, although this is not incorporated into our model. If the disturbance is sufficiently large and/or sufficiently frequent, the landscape might not recover to the preperturbation trajectory. An alternative system might exist, and the disturbance could fundamentally change the nature of the system if the species cannot become reestablished. Subsequently, the landscape might tend to recover along a new and different trajectory."

The flow-kick model of disturbance explores precisely this line of questioning, asking which magnitudes and frequencies of disturbance events are sufficient to push a system to a fundamentally different regime, characterized by different recovery paths. Recent simulation models of landscape disturbance and recovery have also explored the possibility of disturbance-induced regime shifts. For example, Seidl and colleagues[33] investigated the effect of increased fire frequency on forest composition, structure, and function using an individual-based model. Although they did not find evidence of catastrophic shifts, their simulation model showcases a high-resolution and process-based approach for representing interactions between vegetation and disturbances. On the other hand, the flow-kick approach to modeling landscapes uses ODEs to summarize the outcomes of many interacting individuals and processes. Though this modeling choice sacrifices a great deal of resolution, it does enable mathematical analysis of dynamic structures such as alternative stable states without the use of simulations. Thus, in the landscape context, flow-kick models offer strengths complementary to existing models of disturbance.

To illustrate, we apply flow-kick disturbances to a simple model of landscape vegetation cover. The flow-kick landscape model we consider tracks space implicitly as percentage vegetative cover. Kicks reduce this cover by a fixed amount, with the location of vegetation loss unspecified (Supplementary Figure 3d). Kick size, as a percentage of vegetation cover, reflects a combination of disturbance extent and disturbance severity. This coarser treatment of space represents a modeling trade-off that supports a more complex representation of recovery with thresholds and feedbacks, while still allowing mathematical tractability. The flow (recovery) function corresponds to a minimal model of alternative stable states, adapted from Scheffer and colleagues[40] (Supplementary Figure 3e):

$$\frac{dx}{dt} = -a + b(100 - x) - \frac{r(100-x)^2}{(100-x)^2 + h^2}. \qquad \text{(S2.1)}$$

In an interpretation proposed by Scheffer and colleagues[40], the variable x measures the percentage of vegetated land, and $100 - x$ gives percentage of barren soil. The term $-a$

represents loss of vegetative cover (a background destruction and/or mortality rate), $b(100 - x)$ represents

recolonization of bare sites, and $\frac{r(100-x)^2}{(100-x)^2+h^2}$ represents an erosion rate that increases nonlinearly with exposure of bare soil (due, for example, to acceleration of wind and water forces). When vegetative cover exceeds the threshold of 50% (white circle in Supplementary Figure 3e), existing vegetation stabilizes soil sufficiently so that recolonization of bare patches outpaces erosion and mortality, allowing growth to 90% cover (the "vegetated attractor", black circle in Supplementary Figure 3e). However, if vegetative cover falls below 50%, recolonization cannot keep pace with the nonlinear increase in erosion and a different "recovery" trajectory occurs: loss of vegetation until the system re-balances at 13% cover (the "barren attractor", black circle in Supplementary Figure 3e). This contrasts with recovery dynamics in successional patch models, in which patches progress linearly through seral stages (Supplementary Figure 3b). Even

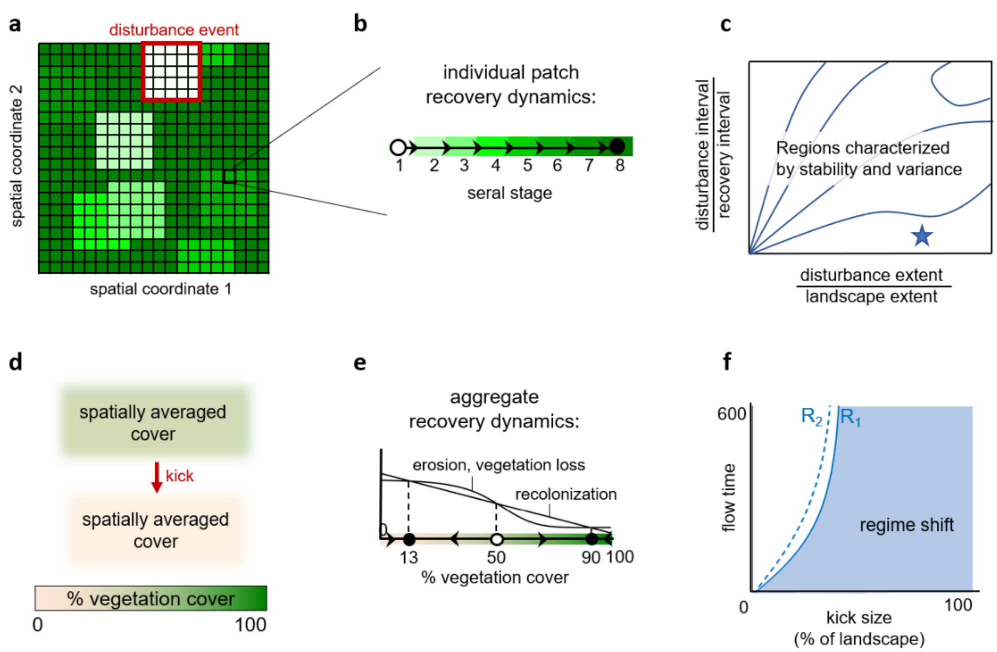

Supplementary Figure 3 | Comparison of successional patch models (a-c) and flow-kick (d-f) landscape models. Panels a, b illustrate model of Turner and colleagues[26]; panel c adapted from ref. [26] Fig. 5. See text for details.

frequent and large disturbances cannot push the successional patch model landscape to an alternate self-reinforcing regime, as subsequent cessation or reduction in disturbances would always allow the landscape to recover to more mature stages. On the other hand, due to nonlinear recovery dynamics in the flow-kick model, a sequence of disturbance events could trigger a regime shift from the basin of the vegetated attractor to the basin of the barren attractor, and subsequent cessation or reduction in disturbances would not allow recovery to the vegetated attractor. Supplementary Table 2 summarizes the similarities and differences between successional patch models and flow-kick models.

Supplementary Figure 3f presents the flow-kick resilience boundary (R_1) between disturbance patterns that cause a regime shift from vegetated to barren and those that allow stabilization of vegetation cover within the vegetated basin of attraction. We have transposed the axes from our usual depiction of disturbance space to highlight the similarity with the phase space of Turner and colleagues[26]. On the horizontal axis, kick size matches normalized disturbance extent; in this landscape flow-kick model that tracks percentage cover, kicks are naturally normalized by the spatial scale of the system. On the vertical axis, flow time matches

Supplementary Table 2 Similarities and differences between flow-kick and successional patch models

<table>
<tr><th>Feature of Model</th><th colspan="2">Flow-Kick Model</th><th>Successional Patch Model</th></tr>
<tr><td>Process of interest</td><td rowspan="4">GENERAL FLOW-KICK</td><td colspan="2">interaction between recovery and disturbance</td></tr>
<tr><td>Results visualized</td><td colspan="2">in a 2D space with disturbance features on axes</td></tr>
<tr><td>Specific to landscapes</td><td>no</td><td>yes</td></tr>
<tr><td>Catastrophic shifts possible</td><td>yes</td><td>no</td></tr>
<tr><td>Vegetation recovery</td><td rowspan="4">LANDSCAPE EXAMPLE</td><td>nonlinear (thresholds, feedbacks)</td><td>linear (monotone succession)</td></tr>
<tr><td>Land patches interact</td><td>yes</td><td>no</td></tr>
<tr><td>Spatial heterogeneity represented explicitly</td><td>no</td><td>yes</td></tr>
<tr><td>Scale normalization</td><td>yes</td><td>yes</td></tr>
</table>

disturbance interval, and could be normalized between landscapes as in [26] by choosing vegetation generation length or another characteristic timescale for units of time. Turner and colleagues[26] speculated that the region of disturbance space corresponding to frequent, large disturbance events (starred in Supplementary Figure 3c) could result in a crash or bifurcation in system structure. The flow-kick model brings this notion to fruition, as the shaded region of flow-kick disturbance space in Supplementary Figure 3f represents disturbance regimes that shift the model system from the basin of the vegetated attractor to the basin of the barren attractor. This shift can be understood as a bifurcation of flow-kick equilibrium intervals (see Supplementary Methods section 7), and would not be reversible by reduction in disturbance.

If we wish to consider vegetation addition instead of destruction, we may choose positive kicks that increase percentage cover. Under this vegetation-addition disruption, flow-kick modeling can also determine a flow-kick resilience boundary for the barren attractor (dashed line, R_2 in Supplementary Figure 3f), with disturbance patterns to the right of the boundary representing planting strategies to trigger a regime shift to the vegetated state.

In summary, flow-kick modeling represents regime shifts and quantifies resilience against those shifts in ways that go beyond successional patch models. On the other hand, successional patch models offer more detailed insight into landscape heterogeneity and variance than is afforded by the flow-kick model considered here. Recent studies that incorporate nonlinear recovery dynamics into spatially explicit landscape simulations[32,33] have taken a step towards combining the strengths of the two modeling approaches. Development of complementary analytic models with greater spatial resolution could yield results of interest in landscape ecology.

2. Critical Slowing Down

Here we contrast the motivation and application range of flow-kick models with those of critical slowing down as an early warning signal for tipping points[48]. Both feature an interplay between disturbances and recovery, but there are two important differences in their assumptions and aims. First, the critical slowing down viewpoint considers a gradual change in some environmental parameter that may eventually cause a bifurcation and uses recovery rates under repeated disturbances to predict closeness to that bifurcation. In contrast, the flow-kick framework probes the dynamics that result from repeated disturbances, not the distance to bifurcation in a slowly changing parameter.

Second, the theory that underpins critical slowing down as an early warning signal for tipping requires that the disturbed state remains sufficiently close to an equilibrium that its recovery rate is well-approximated by the linearization of the system about that equilibrium; the weakening eigenvalues in this linearized system give the slowing down behavior as the system approaches bifurcation. On the other hand, the flow-kick framework makes no assumptions that disturbed states remain close to an underlying equilibrium; its insights hold even when kicks take us far from equilibria and into regions of state space governed by transient dynamics.

Supplementary References

The following sources are also cited in the main article and are reprinted here for convenience.

6. Walker, B. & Salt, D. *Resilience Thinking: Sustaining Ecosystems and People in a Changing World* (Island Press, Washington, D.C., 2006).

18. Turner, M. Disturbance and landscape dynamics in a changing world. *Ecology* **91**, 2833–2849 (2010).

19. Sousa, W.P. The role of disturbance in natural communities. *Ann. Rev. Ecol. Syst.* **15**, 353–391 (1984).

20. White, P.S. & Pickett, STA. Natural disturbance and patch dynamics: an introduction; in Pickett, S.T.A. & White, P.S., eds., *The Ecology of Natural Disturbance and Patch Dynamics* Ch. 1 (Academic Press, New York, 1985).

21. Resilience Alliance. *Assessing Resilience in Social-Ecological Systems: Workbook for Practitioners, Version 2.0*. https://www.resalliance.org/files/ResilienceAssessmentV2_2.pdf (2010).

26. Turner, M.G., Romme, W.H., Gardner, R.H., O'Neill, R.V. & Kratz, T.K. A revised concept of landscape equilibrium: disturbance and stability on scaled landscapes. *Landscape Ecology* **8**, 213–227 (1993).

27. Fraterrigo, J.M. & Rusak, J.A. Disturbance-driven changes in the variability of ecological patterns and processes. *Ecology Letters* **11**, 756–770 (2008).

29. Ippolito, S. & Naudot, V. Alternative stable states, coral reefs, and smooth dynamics with a kick. *Bull. Math Biol.* 10.1007/s11538-016-0148-2 (2016).

30. Ackman, O., Comar, T.D. & Hrozencik, D. On impulsive integrated pest management models with stochastic effects. *Front. Neurosci.* **9**, 10.3389/fnins.2015.00119 (2015).

31. Folke, C. et al. Regime shifts, resilience, and biodiversity in ecosystem management. *Annu. Rev. Ecol. Evol. Syst.* **35**, 557–581 (2004).

32. Daniel, C., Frid, L, Sleeter, B.M. & Fortin, M.J. State-and-transition simulation models: a framework for forecasting landscape change. *Methods Ecol Evol* **7**, 1413–1423 (2016).

33. Seidl, R., Rammer, W., Scheller, R.M. & Spies, T.A. An individual-based process model to simulate landscape-scale forest ecosystem dynamics. *Ecol Modell* **231**, 87–100 (2012).

34. Hirsch, M.W., Smale, S. & Devaney, R.L. *Differential Equations, Dynamical Systems, and an Introduction to Chaos*. Elsevier, Oxford (2013).

40. Scheffer, M., Carpenter, S., Foley, J.A., Folke, C. & Walker, B. Catastrophic shifts in ecosystems. *Nature* **413**, 591–596 (2001).

48. van Nes, E.H. & Scheffer, M. Slow recovery from perturbations as a generic indicator of a nearby catastrophic shift. *Am. Nat.* **169**, 738–747 (2007).